Extraction of Waveguide Scattering Features Using Joint Time-Frequency ISAR

Luiz C. Trintinalia and Hao Ling

Abstract—**A new joint time-frequency ISAR algorithm that combines the conventional ISAR processing with the joint time-frequency signal representation is presented. The adaptive spectrogram, applied to the range axis of the ISAR image, is used as the time-frequency processing engine. The algorithm is tested using the chamber measurement data from a scale model airplane. The results show that the nonpoint scattering mechanisms due to the waveguide-like engine inlet can be seamlessly removed, leading to an enhanced ISAR image consisting only of point scatterers. Furthermore, the extracted inlet features are displayed in the frequency-aspect plane and show distinct waveguide cutoff features.**

I. Introduction

MICROWAVE imaging, in particular inverse synthetic aperture radar (ISAR) imaging, has long been used by the microwave radar community for object diagnostic and target identification applications [1], [2]. ISAR is a simple and very robust process for mapping the position and magnitude of the point scatterers on an object from multifrequency, multiaspect scattered field data. However, complex targets often contain other scattering phenomena such as resonances and dispersive mechanisms, which do not behave like point scatterers. One important example is the scattering from the engine inlet/exhaust duct on an aircraft [3], [4]. It is a dominant contributor to the overall scattering from the target, yet its waveguide-like structure and the associated frequency-dependent scattering mechanisms make it a nonpoint scattering feature. When processed and displayed by the conventional ISAR algorithm, the inlet return results in an image feature that 1) is not well-focused, 2) is not related to the spatial location of the scatterer, and 3) can often obscure other important point features on the target.

It was recently reported that joint time-frequency techniques such as the short-time Fourier transform, Wigner-Ville distribution, and wavelet analysis are very effective means of displaying guided wave mechanisms in electromagnetic backscattered data [5], [6]. The above application of joint time-frequency techniques, however, dealt with single aspect information and did not take advantage of any multiaspect data. In this letter, we present a new processing technique, the joint time-frequency ISAR, that combines the idea of standard ISAR with the joint time-frequency representation of electromagnetic backscattered signals. In our implementation we apply the joint time-frequency technique recently introduced by Qian and Chen [7], called the adaptive spectrogram, to the range (or time) axis of the ISAR image. This technique uses Gaussian basis functions to adaptively parameterize the data and as a consequence, the point scattering mechanisms and resonance phenomena can be readily separated based on the width of the Gaussian bases. The new algorithm is tested using the chamber measurement data from a scaled model airplane. The results show that the nonpoint scattering contribution due to the engine inlet can be seamlessly removed from the ISAR image, leading to a cleaned ISAR image consisting of only point scatterers. The inlet features are best displayed in the frequency-aspect plane and show clear waveguide cutoff features.

Manuscript received June 15, 1995. This work was supported in part by the Joint Services Electronics Program under Contract AFOSR F49620-95-C-0045, NASA Grant NAG3-1589, and CNPq.

L. C. Trintinalia and H. Ling are with the Department of Electrical and Computer Engineering, The University of Texas at Austin, Austin, TX 78712-1084 USA. L. C. Trintinalia is on leave from the Department of Electronic Engineering, Escola Politécnica da Universidade de São Paulo, Brazil.

Publisher Item Identifier S 1051-8207(96)00455-X.

II. Joint Time-Frequency ISAR

We shall describe the conceptual idea behind the joint time-frequency ISAR algorithm. The joint time-frequency processing is first applied to the range (or time) axis of the conventional (range)-(cross range) ISAR image to gain an additional frequency dimension. The result is a three-dimensional (range)-(cross range)-(frequency) matrix, with each (range)-(cross range) slice of this matrix representing an ISAR image at a particular frequency. Consequently, by examining how the ISAR image varies with frequency, we can distinguish the frequency-independent scattering mechanisms from the frequency-dependent ones. In the actual implementation of the joint time-frequency ISAR, the choice of the joint time-frequency processing engine is critical. Our choice is the adaptive spectrogram [7], a signal representation scheme that uses adaptive normalized Gaussian as basis functions. The objective of this method is to expand a signal $s(t)$ in terms of normalized Gaussian functions $h_p(t)$ with an adjustable standard deviation σ_p and a time-frequency center (t_p, f_p)

$$s(t) = \sum_{p=1}^{\infty} B_p h_p(t) \tag{1a}$$

where

$$h_p(t) = (\pi\sigma_p^2)^{-0.25} \exp\left[-\frac{(t-t_p)^2}{2\sigma_p^2}\right] \exp(j2\pi f_p t) \tag{1b}$$

The coefficients B_p are found one at a time by an iterative search procedure. One begins at the stage $p = 1$ by choosing the parameters σ_p, t_p and f_p such that $h_p(t)$ is most "similar"

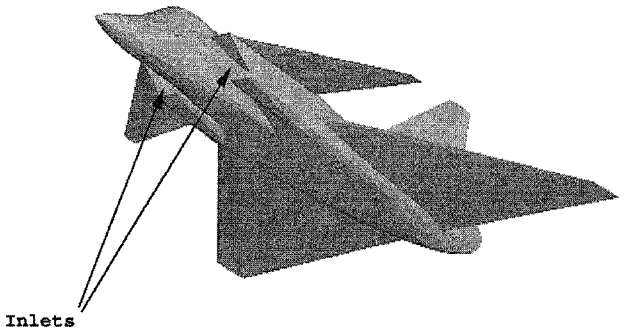

Fig. 1. VFY 218 model.

to $s(t)$, i.e., for which the inner product between $s(t)$ and $h_p(t)$ is the largest. The next B_p is found using the same procedure after the orthogonal projection of $s(t)$ onto $h_p(t)$ has been removed from the signal. This procedure is iterated to generate as many coefficients as needed to accurately represent the original signal. The details of this iterative algorithm can be found in [7].

The adaptive spectrogram has two distinct advantages over conventional time-frequency techniques such as the short-time Fourier transform. First, it is a parameterization procedure that results in very high time-frequency resolution. More importantly for our application, the adaptive spectrogram allows us to automatically distinguish the frequency-dependent events from the frequency-independent ones through the extent of the basis functions. From (1b) it can be seen that scattering centers, i.e., signals with very narrow length in time, will be well represented by basis functions with very small σ_p. Frequency resonances, on the other hand, will be better depicted by large σ_p. Therefore, if we reconstruct the ISAR image using only those Gaussian bases with small variances, a much "cleaner" image can be obtained showing only the scattering centers. The remaining mechanisms, i.e. those related to the large variance Gaussians, are more meaningful to view in a dual frequency-aspect display where resonances and other frequency-dependent mechanisms can be better identified. Finally, we should point out that to obtain the adaptive Gaussian representation requires additional computational expense. However, the resulting representation is highly parsimonious and allows additional insight into the scattering features.

III. Results

The algorithm is demonstrated using the chamber measurement data of a 1 : 30 scale model Lockheed VFY-218 airplane provided by the EMCC (Electromagnetic Code Consortium) [8]. The airplane has two long engine inlet ducts, as shown in Fig. 1, which are rectangular at the open ends but merge together into one circular section before reaching a single-compressor face. As we can clearly see in the conventional ISAR image of Fig. 2 for the vertical polarization at 20° near nose-on, the large cloud outside the airframe structure is the inlet return. Fig. 3 shows the enhanced ISAR image of Fig. 2, obtained by applying the above joint time-frequency ISAR algorithm (329 basis functions were used to represent the whole ISAR image) and keeping only the small variance Gaussians. We see that only the scattering center part of the

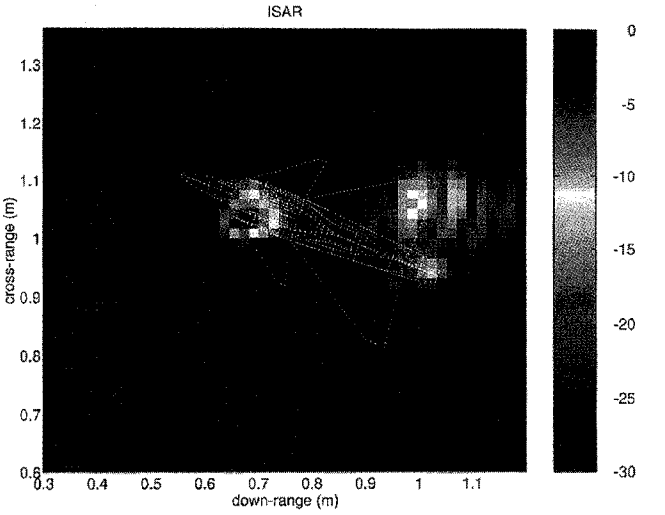

Fig. 2. ISAR image of VFY 218 model.

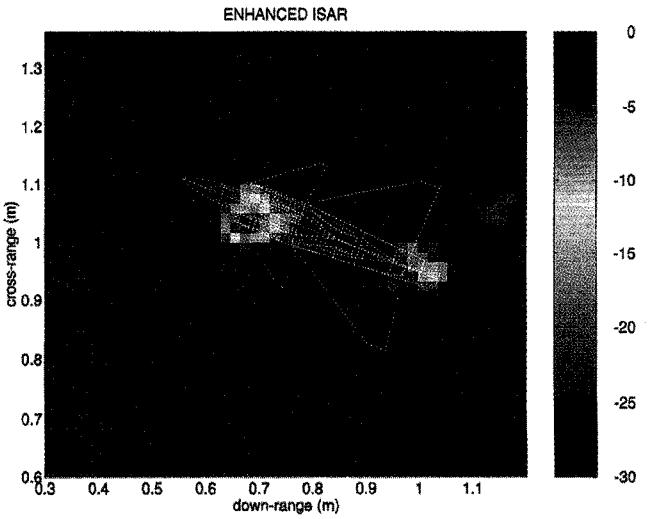

Fig. 3. Enhanced ISAR image of VFY 218 model.

original signal remains in the image, as expected. Notice that the strong return due to engine inlet has been removed, but the scattering from the tail fin remains. Fig. 4 shows the frequency-aspect display of the high variance Gaussians. A number of equispaced vertical lines can be seen between 10.5 and 13.5 GHz. Given the dimension of the rectangular inlet opening (approximately 1.5 cm × 2.5 cm), we estimate that these frequencies correspond approximately to the cutoff frequencies of the higher-order modes in the waveguide-like inlet. We have also run our algorithm on the simulated scattering data, generated using a numerical Maxwell's solver, for a plate-waveguide configuration to verify this claim. The frequency resonances displayed indeed correspond very closely to the theoretical cutoff frequencies of the waveguide.

IV. Conclusion

In this letter we presented a new joint time-frequency ISAR algorithm to process data from complex targets containing not only scattering centers but also other frequency-dependent scattering mechanisms. The adaptive joint time-

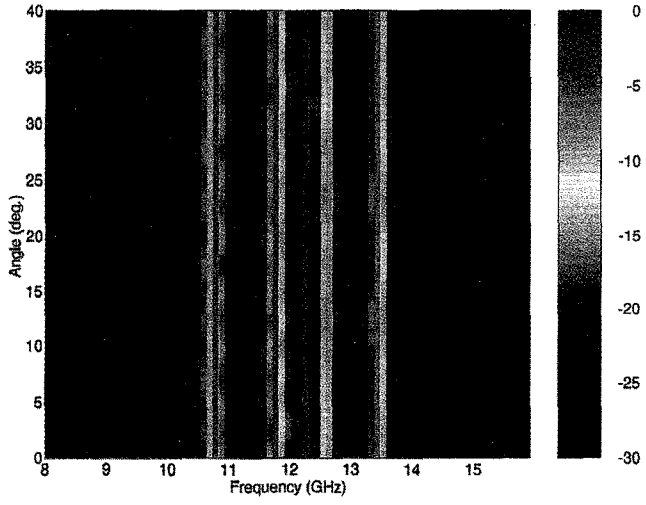

Fig. 4. Frequency-aspect plot showing the inlet resonances extracted from the ISAR image of the VFY 218 model.

frequency ISAR algorithm allows the enhancement of the ISAR image by eliminating nonpoint scatterer signals, thus leading to a much cleaner ISAR image. It also provides information on the extracted frequency-dependent mechanisms such as resonances and frequency dispersions. This is accomplished without any loss in resolution.

ACKNOWLEDGMENT

The United States Government is authorized to reproduce and distribute reprints for governmental purposes notwithstanding any copyright notation hereon.

REFERENCES

[1] D. L. Mensa, *High Resolution Radar Imaging.* Dedham, MA: Artech House, 1981.

[2] N. H. Farhat, C. L. Werner, and T. H. Chu, "Prospects for three-dimensional projective and tomographic imaging radar networks," *Radio Sci.*, vol. 19, pp. 1347–1355, Sept.-Oct. 1984.

[3] H. Ling, R. Chou, and S. W. Lee, "Shooting and bouncing rays: Calculating the RCS of an arbitrary shaped cavity," *IEEE Trans. Antennas Propagat.*, vol. 37, pp. 194–205, Feb. 1989.

[4] P. H. Pathak and R. J. Burkholder, "A reciprocity formulation for the EM scattering by an obstacle within a large open cavity," *IEEE Trans. Microwave Theory Tech.*, vol. 41, pp. 702–707, Apr. 1993.

[5] A. Moghaddar and E. K. Walton, "Time-frequency-distribution analysis of scattering from waveguide cavities," *IEEE Trans. Antennas Propagat.*, vol. 41, pp. 677–680, May 1993.

[6] H. Ling and H. Kim, "Wavelet analysis of backscattering data from an open-ended waveguide cavity," *IEEE Microwave and Guided Wave Lett.*, vol. 2, pp. 140–142, Apr. 1992.

[7] S. Qian and D. Chen, "Signal representation using adaptive normalized Gaussian functions," *Signal Processing*, vol. 36, pp. 1–11, Mar. 1994.

[8] H. T. G. Wang, M. L. Sanders, and A. Woo, "Radar cross section measurement data of the VFY 218 configuration," Tech. Rep. NAWCWPNS TM-7621, Naval Air Warfare Center, China Lake, CA, Jan. 1994.